ELSEVIER

Molecular and electronic structure of (η⁵-pentaalkyl-2,3-dihydro-1,3-diborolyl) (η⁵-pentamethylcyclopentadienyl)metal complexes, M = Fe, Ru

Isabella Hyla-Kryspin [b],[*], Yong Nie [a], Hans Pritzkow [a], Walter Siebert [a],[*]

[a] *Anorganisch-Chemisches Institut der Universität Heidelberg, Im Neuenheimer Feld 270, 69120 Heidelberg, Germany*
[b] *Institut für Organische Chemie der Universität Münster, Corrensstr. 40, D-48149 Münster, Germany*

Dedicated to Professor Mike Mingos.

Abstract

The X-ray diffraction study of the violet ruthenium sandwich derivative **2b** revealed a folding along the B···B vector of the 1,3-diborolyl heterocycle of 40.7°, which is very similar to that in the green iron complex **1b**. The molecular and electronic structure of the 1,3-diborolyl complexes of iron and ruthenium have been studied by density functional theory (DFT) with the B3LYP functional and extended triple-ζ basis sets. It is shown that the folding of the diborolyl ligand in the title complexes is due to electronic factors. The model complexes with a planar diborolyl ligand **1′** (M = Fe) and **2′** (M = Ru) are by 24.9 and 24.5 kcal/mol less stable than the equilibrium folded structures of **1** and **2**, respectively. The electronic structures of **1** and **2** show similarities to those of the 18 VE species due to the participation of the σ(B–C2) bonds in the stabilizing diborolyl–metal bonding. The electronic spectra of **1** and **2** have been studied with the time-dependent DFT method. The absorptions observed in the visible range in the electronic spectrum of the title complexes are assigned as spin-allowed d–d transition with an admixture of metal to diborolyl (π^*) charge transfer (MLCT).
© 2006 Elsevier B.V. All rights reserved.

Keywords: Boron; Heterocycle; Iron; Ruthenium; Complexes; DFT calculation

1. Introduction

Electron-poor organometallic compounds of the iron triad have interesting electronic structures and reactivities. We have studied the formally 16 VE sandwich **1b** [1a,1b] [(η⁵-C₅Me₅)Fe(η⁵-(C^{i}Pr)₂(BEt)₂CMe)] and more recently, its analogous (η⁵-pentaalkyl-2,3-dihydro-1,3-diborolyl)(η⁵-pentamethylcyclopentadienyl)ruthenium complexes **2** [2]. The unique structural feature of the green iron complex **1b** is its severe folding of the diborolyl ring along the B···B vector (folding angle α = 41.3°) as a result of a strong Fe–C2 bond (1.899 Å) and the additional interaction of the

high-lying combination of σ(B–C) orbitals with the empty d$_{xz}$ orbital of iron. This bonding pattern allows 5e of the (neutral) folded 1,3-diborolyl ring to interact with the metal, which is markedly different from less folded 1,3-diborolyl ligands functioning as 3e donors. According to spectroscopic data, the violet ruthenium analogs **2** [2] are assumed to have a similar bonding situation, however, the difficulty [3] in obtaining suitable crystals has hampered the determination of a detailed structure. Its reactivity e.g. the formation of classic 18 VE complexes with a decreased folding of the heterocycle has been studied by coordination of the donor molecules :CO and :CN–R at the Ru center which yields yellow complexes **3** with folding angles <20° along the B···B vector of the heterocycles [1b,2a]. Phosphanes and **2** also form donor–acceptor complexes **2 · PH₂R** (R = H, Ph), whereas triorganylphosphane adducts **2 · PR₃** (R = Me, Ph) are

---

* Corresponding authors. Fax: +49 6221 545609 (W. Siebert).
  E-mail addresses: ihk@uni-muenster.de (I. Hyla-Kryspin), walter.siebert@urz.uni-heidelberg.de (W. Siebert).

unstable. Terminal alkynes insert into one of the B–C–B bonds to give the novel 18 VE η^7-4-borataborepine complexes **4** in which the (anionic) seven-membered ring functions as 6e ligand [4]. With internal alkynes the formation of boratabenzene complexes occurs, and preliminary results have been communicated. Here we report on the details of the crystal and electronic structures of the violet sandwiches **2** in comparison to those of green **1**.

1b   **2**

3   **4**
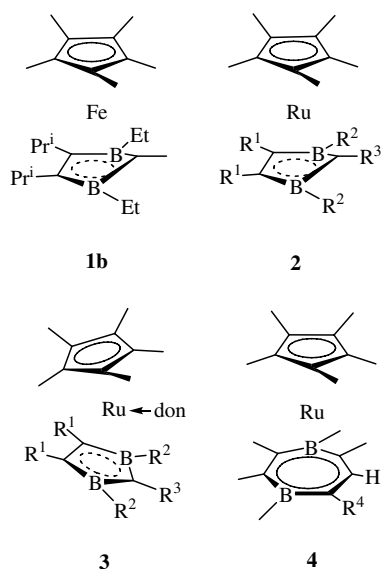
2. Results and discussion

2.1. Crystal structure of the bis-trimethylsilylmethyl derivative 2b

We have been trying for years to obtain the detailed structure of a derivative of (η^5-pentaalkyl-2,3-dihydro-1,3-diborolyl)(η^5-pentamethylcyclopentadienyl)ruthenium complexes **2** to further understand its unique properties. Finally, compound **2b** [2a], first isolated as a dark violet oil, on cooling in hexane gave suitable crystals for an X-ray structure analysis. Its structure (Fig. 1) confirms that the 1,3-diborolyl ring is folded by 40.7° along the B···B vector, very similar to its green iron analog **1b**. The Ru–C2 bond length (2.029, cf. Fe–C2 1.899 Å) is markedly shorter than the other Ru–C bond lengths to the heterocycle. Upon coordination of a donor ligand such as Me$_3$CNC the folding angle along the B···B vector is reduced to 16.2°/19.0° [1b,2a].

2.2. Electronic structures of the model complexes of iron 1 and ruthenium 2

Some years ago the electronic structure of complex **1** was investigated with the help of semiempirical Extended-Hückel calculations [1b]. On the basis of the qualitative interaction diagrams and the comparison with bonding properties of the cyclopentadienyl ligand as well as the 18 VE rule it was possible to postulate that the folding of the diborolyl
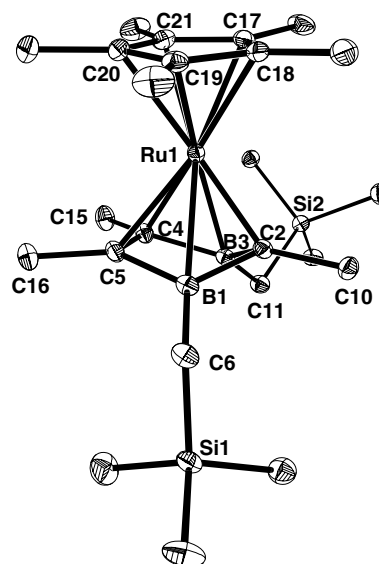

Fig. 1. Molecular structure of **2b**, hydrogen atoms have been omitted for clarity. Selected bond lengths (Å) and bond angles (°): Ru1–Cp* 2.139(2)–2.219(2), Ru1–C2 2.029(2), Ru1–B1 2.359(2), Ru1–C5 2.225(2), Ru1–C4 2.221(2), Ru1–B3 2.405(3), B1–C5 1.574(3), C4–C5 1.399(3), B3–C4 1.582(3), B3–C2 1.560(3), B1–C2 1.559(3) and C2–B1–C5 109.7(2), C4–C5–B1 105.8(2), C5–C4–B3 103.8(2), C2–B3–C4 109.6(2), B1–C2–B3 90.1(2).

ligand of complex **1** is due to electronic factors. It is clear that a more accurate and quantitative description of the structural and electronic properties of complex **1** could not be achieved within the Extended-Hückel scheme. Nowadays, computational transition metal chemistry is dominated by density functional theory (DFT) approaches [5] which are able to provide good results not only for geometries and the energetics but also for spectroscopic properties of the investigated species. Up to now, alternative high level *ab initio* methods are either too costly for large molecules or not accurate enough.

The investigation has been continued on complex **2** as well as on **1** with the DFT/B3LYP method [6] as described in Section 4.2. We started with geometry optimizations for
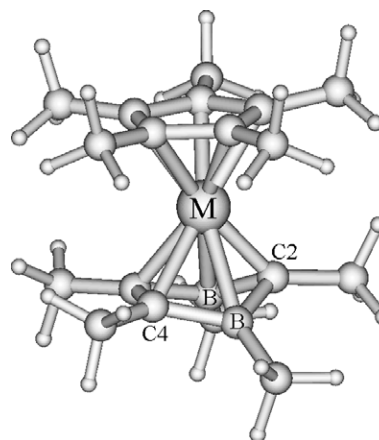

Fig. 2. Optimized structure of the decamethyl model complexes **1a** (M = Fe) and **2a** (M = Ru).

the decamethyl model complexes **2a** and **1a** without symmetry constraints. Both optimized structures converged to C_s-symmetrical species (Fig. 2).

In order to investigate the possible influence of the substituents on structural and electronic properties of the complexed ligands we continued with B3LYP calculations on the (folded) model complexes **2**, **1** and the (planar) **2′** and **1′** as well as on the free 1,3-diborolyl anion (**5′**-H)⁻ and the metal complex fragments Fe(C₅H₅)⁺ and Ru(C₅H₅)⁺. In the model complexes **1** and **2** the substituents on both ligands are hydrogen atoms. During the geometry optimization for **1′** and **2′** we required a planar structure of the diborolyl ligand (constrained geometry optimizations) (Fig. 3). The calculations for **1**, **1′** and **2**, **2′** were carried out under the C_s-symmetry constraint. We are interested in (i) structural, electronic and energetic properties of the optimized structures, (ii) bonding energies of the diborolyl ligand, and (iii) spectroscopic properties of the optimized minimum structures.

Selected optimized parameters of **1a** and **2a** are compared with the X-ray data of **1b** and **2b** in Table 1, and those of **1**, **1′** and **2**, **2′** are collected in Table 2.

From Tables 1 and 2 it is evident that the B3LYP optimized parameters corresponding to the gas-phase structures of the model complexes **1**, **1a** and **2**, **2a** agree well with the values determined experimentally for the solid **1b** and **2b**, respectively. The bond lengths of **1** and **2** optimized with basis sets containing polarization functions (BS1) are closer to the corresponding experimental values than those of the decamethyl model compounds **1a** and **2a** optimized with basis sets without polarization functions (BS2) (Tables 1 and 2). Since this discrepancy suggests that polarization functions are important for accurate geometry optimizations of the investigated complexes, we reoptimized **1a** and **2a** with basis set BS1. From Table 1 it is evident that the addition of polarization functions to the basis sets improve the accuracy of the optimized bond lengths of **1a** and **2a**.

The folding of the diborolyl ring along the B···B vector, α, in the optimized structures of the model complexes **1a** [39.6° (BS2), 39.8° (BS1)], **1** [41.1° (BS1)], **2a** [40.8° (BS2), 40.4° (BS1)] and **2** [41.7° (BS1)] agrees very well with the experimental value of **1b** (41.3°) and **2b** (40.7°). The optimized values α suggests that the folding of the diborolyl
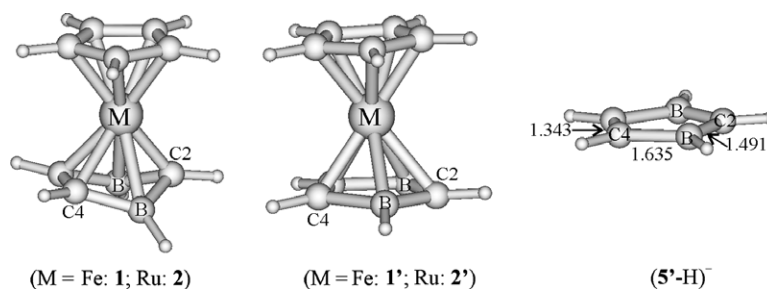

Fig. 3. Optimized structures of the model complexes **1**, **2** and the free 1,3-diborolyl anion (**5′**-H)⁻.

Table 1
Comparison of selected optimized parameters of the model complexes **1a** and **2a** with X-ray data of **1b** and **2b**

| Distance (Å)	M = Fe			M = Ru		
	Calc. (**1a**)		Exp. (**1b**)	Calc. (**2a**)		Exp. (**2b**)
	BS2	BS1	X-ray [1a]	BS2	BS1	X-ray
M–C(Cp)avr	2.122	2.093	2.054–2.118	2.228	2.220	2.138–2.219(2)
M–C2	1.936	1.931	1.899(4)	2.041	2.040	2.029(2)
M–C4	2.143	2.127	2.116(3)	2.247	2.251	2.223(2)
M–B	2.288	2.266	2.248(4)	2.399	2.399	2.382(3)
B–C2	1.562	1.550	1.547(6)	1.567	1.562	1.559(3)
B–C4	1.578	1.575	1.568(5)	1.581	1.577	1.578(3)
C4–C5	1.404	1.393	1.412(6)	1.406	1.398	1.399(3)
α (°)[a]	39.6	39.8	41.3	40.8	40.4	40.7

[a] Folding of the diborolyl ring along the B···B vector
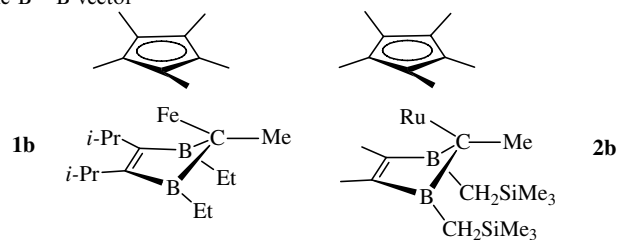
Table 2
Relative energies, number of imaginary frequencies (NIMAG), and selected optimized parameters of the model complexes **1** and **2**

	1 (C_s)	**1′** (C_s)	**2** (C_s)	**2′** (C_s)
E_{rel} (kcal/mol)	0.00	+24.9	0.00	+24.5
NIMAG	0	3	0	3
Distance (Å)				
M–C(Cp)$_{avr}$	2.091	2.065	2.227	2.190
M–C2	1.906	2.207	2.016	2.371
M–C4	2.096	2.084	2.221	2.252
M–B	2.251	2.150	2.382	2.314
B–C2	1.545	1.507	1.556	1.513
B–C4	1.565	1.667	1.566	1.652
C4–C5	1.390	1.357	1.395	1.362
α (°)[a]	41.1	0.0	41.7	0.0

[a] Folding of the diborolyl ring along the B···B vector.

ligand in **1b** and **2b** is not due to steric factors. Taking into account the computational cost as well as the fact that the most important geometrical features od **1b** and **2b** are good reproduced by the calculations, in the following we discuss the properties of **1** and **2** in more details. The optimized structures **1** and **2** represent minima, while **1′** and **2′** do not correspond to stationary points on the potential energy surfaces. According to the vibrational analyses all frequencies are real for **1** and **2** while for **1′** and **2′** three imaginary modes were found (Table 2). The free diborolyl anion (**5′**-H)⁻ adopts a planar structure (Fig. 3). The transformation of the free diborolyl ligand from the equilibrium structure (**5′**-H)⁻ into the folded geometry (**5**-H)⁻, i.e., into the geometry which it adopts in the complexes **1** and **2**, destabilizes the free ligand by 11.4 and 12.6 kcal/mol, respec-

tively. However, with respect to **1′** and **2′** the equilibrium folded structures **1** and **2** are by 24.9 and 24.5 kcal/mol more stable (Table 2). The M–C2 distance of **1** (1.906 Å) and **2** (2.016 Å) is significantly shorter than in the sandwiches **1′** (2.207 Å) and **2′** (2.371 Å). Upon going from (**5′**-H)⁻ to **1** and **2** an elongation of the C4–C5 and B–C2 bonds is observed. The C4–C5 bond distance increases from 1.343 (**5′**-H)⁻ to 1.390 (**1**) and 1.395 Å (**2**). With respect to (**5′**-H)⁻ the B–C2 bonds are stretched by 0.054 (**1**) and 0.065 Å (**2**) (Table 2). It is clear that the elongation of the B–C2 bonds in the complexed diborolyl ligand weakens these σ bonds and facilitates the insertion of alkynes.

The binding energy of the free diborolyl ligand (**5′**-H)⁻ with the metal fragments Fe(C₅H₅)⁺ and Ru(C₅H₅)⁺ to give the complexes **1** and **2** amounts to 216.4 and 196.4 kcal/mol,
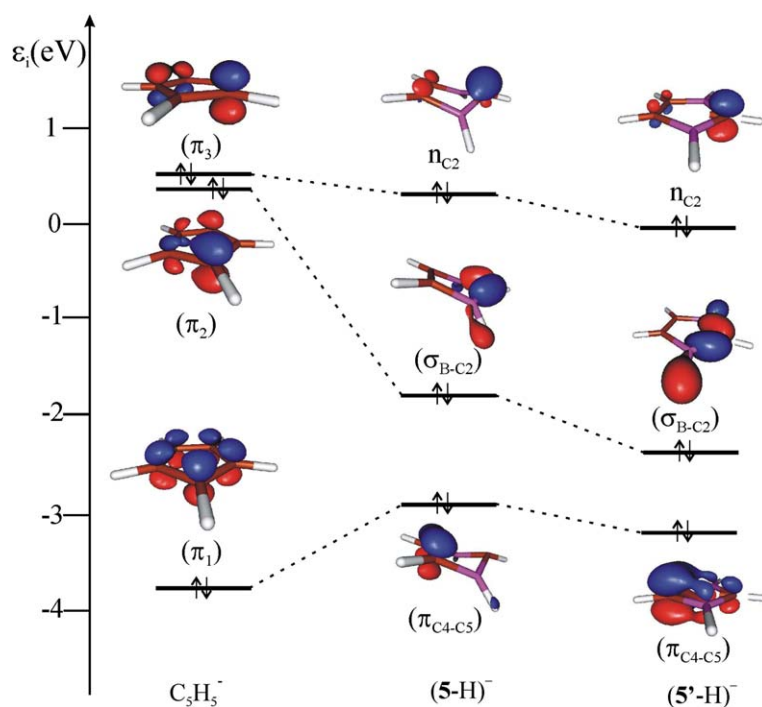

Fig. 4. Comparison of the highest occupied Kohn–Sham MOs of the free diborolyl ligand in the optimized (**5′**-H)⁻ and folded (**5**-H)⁻ geometry with those of C₅H₅⁻.
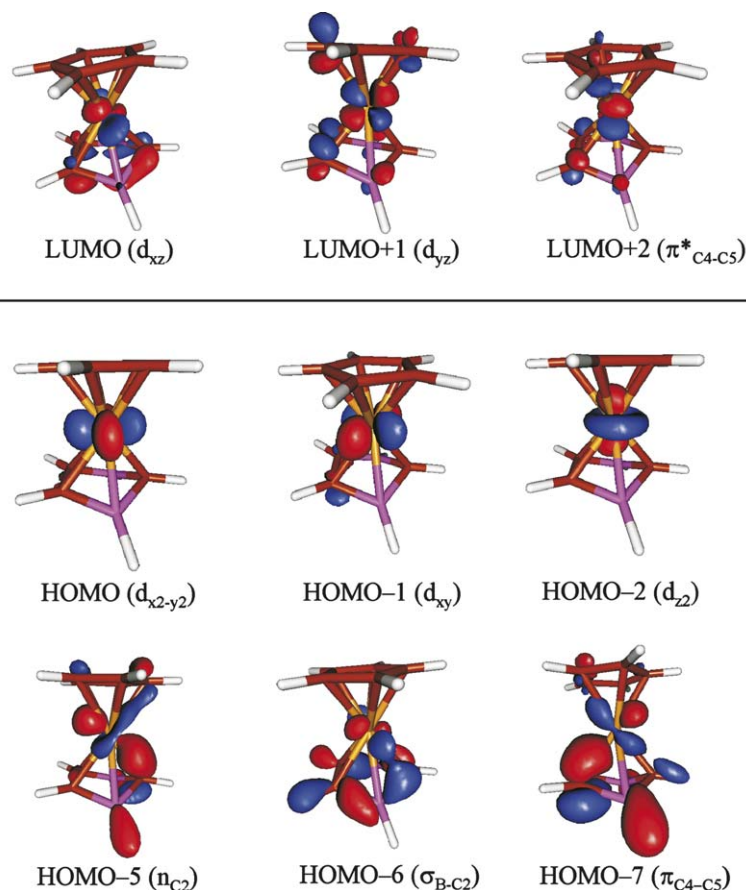
Fig. 5. Valence Kohn–Sham MOs of **1** and **2** with predominant metal and diborolyl character.

respectively. To further explore the bonding properties of the diborolyl ligand in Fig. 4 we compare the highest occupied Kohn–Sham MOs of the planar $(5'\text{-H})^-$ and folded $(5\text{-H})^-$ structures with those of the cyclopentadienyl anion, $C_5H_5^-$. It is well known that the bonding properties of $C_5H_5^-$ are inherently connected with the ability of its π_1, π_2, and π_3 MOs to act as electron density donors to the empty metal levels [7]. With respect to $C_5H_5^-$ the diborolyl anion lacks two π electrons and consequently **1** and **2** are classified as 16 VE species. However, from the comparison of the MO shapes in Fig. 4 it follows that in addition to the $\pi(\text{C4–C5})$ and $n(\text{C2})$ MOs the high-lying $\sigma(\text{B–C2})$ orbital can also be involved in the diborolyl–metal bonding. An examination of the valence Kohn–Sham MOs of **1** and **2** confirms the close similarity with the electronic structures of the parent 18 VE species (Fig. 5).

Thus, similar to ferrocene or ruthenocene the three highest occupied MOs of **1** and **2** can be characterized as metal "t_{2g}"-like level and LUMO with LUMO + 1 as the empty "e_g" set (Fig. 5) [7]. According to the DFT wave functions of **1** and **2**, the HOMO − 5, HOMO − 6, and HOMO − 7 describe the possible donor–acceptor interactions between diborolyl $n(\text{C2})$, $\sigma(\text{B–C2})$, and $\pi(\text{C4–C5})$ MOs and the d_{xz}- and d_{yz}-like empty metal levels (Fig. 5). For the sake of clarity, the MOs with predominant cyclopentadienyl π character are omitted in Fig. 5.

In general, the strength of donor–acceptor interactions may be quantified with help of NBO population analyses [8]. As an example in Table 3 we compare the second-order perturbative estimates of the stabilizing energy $[E(2)]$ associated with delocalization of electron density from diborolyl donor NBOs to the acceptor Ru NBOs (L.p.* Ru) calculated for **2** and **2'**. From Table 3 it is evident that the folding of the diborolyl ligand make all these interactions stronger. Furthermore, upon going from **2'** to **2** a decrease of the electron population of the $\sigma(\text{B–C2})$ NBO is observed [1.996e (**2'**) vs. 1.773e (**2**)]. This decrease of electron populations nicely correlates with the elongation of the B–C2 bonds in **2** with respect to those of **2'** (Table 2). Although the formal electron count yields a 16 valence electrons for **1** and **2**, the participation of the $\sigma(\text{B–C2})$

Table 3
Second-order perturbative stabilizing energy $[E(2)]$ of donor–acceptor interactions between occupied diborolyl and empty Ru NBOs calculated for **2** and **2'**

Interaction	$E(2)$ (kcal/mol)	
	2	**2'**
$\pi(\text{C4–C5}) \rightarrow$ L.p.* Ru ($4d_{yz}$)	183.5	100.6
$n(\text{C2}) \rightarrow$ L.p.* Ru ($5s + 4d_{yz}$)	66.4	21.6
$\sigma(\text{B–C2}) \rightarrow$ L.p.* Ru ($4d_{xz}$)	41.9	17.9

Table 4
TD-DFT calculated excitation energies (ΔE) and assignments for the five lowest excited singlet states of the model complexes **1** and **2**

Complex	ΔE			Excited state	Leading orbital excitations	Character[b]
	(nm)	(eV)	f^a			
1	1059	1.17	0.0007	1A″	0.57 HOMO → LUMO	d → d
					0.15 HOMO → LUMO + 2	d → d
	850	1.46	0.0035	1A′	0.56 HOMO − 1 → LUMO	d → d
					0.24 HOMO − 1 → LUMO + 2	d → L : π^*_{C4-C5}
	751	1.65	0.0000	2A″	0.58 HOMO − 2 → LUMO	d → d
					0.24 HOMO − 2 → LUMO + 2	d → L : π^*_{C4-C5}
	453	2.73	0.0005	2A′	0.58 HOMO → LUMO + 1	d → d
					0.31 HOMO − 2 → LUMO + 1	d → d
	405	3.06	0.0011	2A″	0.59 HOMO − 1 → LUMO + 1	d → d
					0.26 HOMO → LUMO + 2	d → L : π^*_{C4-C5}
2	634	1.95	0.0021	1A″	0.65 HOMO → LUMO	d → d
					0.11 HOMO − 2 → LUMO	d → d
	622	1.99	0.0017	2A″	0.65 HOMO − 2 → LUMO	d → d
					0.13 HOMO − 2 → LUMO + 2	d → L : π^*_{C4-C5}
	552	2.45	0.0087	1A′	0.64 HOMO − 1 → LUMO	d → d
					0.13 HOMO − 1 → LUMO + 2	d → L : π^*_{C4-C5}
	385	3.22	0.0024	3A″	0.68 HOMO − 3 → LUMO	Cp: π_3 → d
	313	3.96	0.0000	2A′	0.53 HOMO → LUMO + 1	d → d
					0.37 HOMO − 2 → LUMO + 1	d → d

[a] Oscillator strength.
[b] L = diborolyl, Cp = C_5H_5.

MO in the diborolyl–metal bonding suggests an effective 18 VE configuration.

Finally we have studied the vertical excitation energies for the 10 lowest excited states of **1** and **2** by using the time-dependent DFT method (TD-DFT) [9]. These excited states predict spin-allowed electronic transition in the energy regions 1059–310 nm (**1**) and 634–281 nm (**2**). The character of the particular electronic transitions is analyzed in terms of contributing orbital excitation and the calculated oscillator strengths. In the electronic spectra of **1b** and **2b** an absorption in the visible range [750–800 nm (1.65–1.55 eV) (**1b**); 560–580 nm (2.21–2.14 eV) (**2b**)] was detected [10]. Table 4 contains the calculated energies for the five lowest excited states of **1** and **2** together with oscillator strengths and the character of the leading one-electron excitation. The calculated excitation to the 1A′ singlet state of the model complexes **1** [850 nm (1.46 eV)] and **2** [552 nm (2.45 eV)] agrees reasonably well with the experimental spectra of **1b** and **2b**. Both excitations can be generally assigned as spin-allowed d–d transitions but with the admixture of metal to ligand charge transfer (MLCT). The transitions to the 2A′ singlet state of **1** at 453 nm and **2** at 313 nm have pure d–d character (Table 4). It is interesting to note that these transitions nicely correlate with the low-intensity bands in the spectrum of ferrocene and ruthenocene at 441 and 323 nm, respectively, which are known to result from spin-allowed d–d excitations [11].

3. Conclusion

In conclusion, we have shown the unique structural and bonding properties of the electron-poor 1,3-diborolylruthenium complexes **2** by a combination of X-ray structure

analysis and DFT calculations. The optimized global minimum structure of the model ruthenium complexes **2** and **2a** as well as of their iron analogs **1** and **1a** reproduce very well the folded structure of the complexed diborolyl ligand. The folding of the diborolyl ligand is due to donor–acceptor interactions between the σ(B–C2) MOs and the empty metal levels which in the folded structures (**1** and **2**) are stronger than in the planar (**1′** and **2′**) ones. Although for the investigated 1,3-diborolyl complexes the formal electron count predict a 16 VE configuration the contribution from σ(B–C2) MO to the diborolyl–metal bonding suggests an effective 18 VE configuration similar to that of ferrocene and ruthenocene. The absorption observed in the visible range of the electronic spectra of the title compounds are assigned as spin-allowed d–d transition with an admixture of metal to ligand (π^*_{C4-C5}) charge transfer (MLCT).

4. Experimental

4.1. X-ray structure analysis of 2b

Intensity data were collected on a Bruker AXS SMART CCD diffractometer at $T = 103$ (2) K. Mo Kα radiation, $\lambda = 0.71073$ Å, graphite monochromator, ω-scans. The structure was solved by direct methods and refined by least-squares methods based on F^2 with all measured reflections, all non-hydrogen atoms are refined anisotropically [12]. monoclinic, space group $P2_1/c$, $C_{24}H_{46}B_2RuSi_2$, $a = 18.7559(8)$ Å, $b = 8.9859(4)$ Å, $c = 18.0098(8)$ Å, $\beta = 114.131(1)°$, $V = 2770.1(2)$ Å^3, $Z = 4$, $D_c = 1.231$ g cm^{-3}; 38 020 reflections ($\theta_{max} = 32°$) collected, 9545 independent reflections [$R_{int} = 0.0539$]. $R_1 = 0.0338$ ($I > 2\sigma(I)$), $wR_2 = 0.0823$ (all data). CCDC-244072 contains the supplemen-

tary crystallographic data for this paper. These data can be obtained free of charge via www.ccdc.cam.ac.uk/conts/retrieving.html (or from the Cambridge Crystallographic Data Centre, 12, Union Road, Cambridge CB2 1EZ, UK; fax: +44 1223 336 033 or deposit@ccdc.cam. ac.uk).

4.2. Computational details

All DFT calculations have been carried out with the GAUSSIAN 98 program [13] by using the B3LYP functional [6]. For the iron complexes an all-electron basis set was used. In the case of **1** and **1′** the Fe atom was described by Wachters (14s,9p,5d)/[9s,5p,3d] basis [14] augmented with one 4f polarization function ($\alpha_f = 1.05$) and the standard 6-311G∗ basis sets were used for the remaining atoms [15]. The polarization functions in these basis sets were initially omitted in the calculations on **1a**. For the ruthenium complexes **2** and **2′** we have used the TZVP basis sets from the TURBOMOLE basis set library: (11s,6p,1d)/[5s,3p,1d] for C and B, (5s,1p)/[3a,1p] for H, and (7s,6p,5d,1f)/[5s,3p,3d,1f] for the valence electrons of Ru [16]. The 28 core electrons of Ru were approximated by quasirelativistic pseudopotentials [17]. The calculations on **2a** were first carried out without polarization functions in the basis sets of Ru and H. The basis sets containing polarization functions for all atoms are denoted as BS1 and those without polarization functions as BS2. Geometry optimizations were carried out by using analytical gradient procedures. The presented structures correspond to fully converged geometries with gradients and displacement below the thresholds implemented in GAUSSIAN 98. To check the importance of polarization functions on geometry optimizations the B3LYP/BS2 structures of **1a** and **2a** were reoptimized by using the basis sets BS1. Vibrational frequencies were obtained from analytic calculation of the Hessian matrices. Vertical excitation energies were studied by the TD-DFT [9] method with the same functional and basis sets as described above. In the NBO population analyses [8] the second-order perturbative stabilizing energy [$E(2)$] associated with donor–acceptor interactions was calculated according to the following equation:

$$E(2) = n_i F_{ij}^2 : (\varepsilon_j - \varepsilon_i),$$

where n_i is the donor orbital occupancy, ε_i and ε_j are diagonal elements corresponding to energies of the donor(i) and acceptor(j) NBOs, and F_{ij} is the off-diagonal Fock matrix element in the NBO basis. For graphical displays we have used the MOLDEN program [18].

Acknowledgements

References

[1] (a) W. Siebert, R. Hettrich, H. Pritzkow, Angew. Chem. 106 (1994) 215–217;
W. Siebert, R. Hettrich, H. Pritzkow, Angew. Chem., Int. Ed. Engl. 33 (1994) 203–204;
(b) R. Hettrich, M. Kaschke, H. Wadepohl, W. Weinmann, M. Stephan, H. Pritzkow, W. Siebert, I. Hyla-Kryspin, R. Gleiter, Chem. Eur. J. 2 (1996) 487–494.
[2] (a) T. Müller, M. Kaschke, M. Strauch, A. Ginsberg, H. Pritzkow, W. Siebert, Eur. J. Inorg. Chem. (1999) 1685–1692;
(b) B. Bach, Y. Nie, H. Pritzkow, W. Siebert, J. Organomet. Chem. 689 (2004) 429–437.
[3] (a) M. Kaschke, Ph.D. Thesis, Universität Heidelberg, 1995;
(b) T. Müller, Ph.D. Thesis, Universität Heidelberg, 1999;
(c) B. Bach, Ph.D. Thesis, Universität Heidelberg, 2003.
[4] (a) Y. Nie, H. Pritzkow, C.-H. Hu, T. Oeser, B. Bach, T. Müller, W. Siebert, Angew. Chem. 117 (2005) 638–640;
(b) Y. Nie, H. Pritzkow, C.-H. Hu, T. Oeser, B. Bach, T. Müller, W. Siebert, Angew. Chem. Int. Ed. 44 (2005) 632–634.
[5] G. Frenking, T. Wagener, in: P.v.R. Schleyer (Ed.), Encyclopedia of Computational Chemistry, Wiley, New York, 1998, pp. 3073–3084.
[6] (a) A.D. Becke, J. Chem. Phys. 98 (1993) 5648–5652;
(b) S.H. Vosko, L. Wilk, M. Nusair, Can. J. Phys. 58 (1980) 1200–1211;
(c) C. Lee, W. Yang, R.G. Parr, Phys. Rev. B 37 (1988) 785–789.
[7] T.A. Albright, J.K. Burdett, M.-H. Whangbo, Orbital Interactions in Chemistry, Wiley, New York, 1985.
[8] (a) J.P. Foster, F. Weinhold, J. Am. Chem. Soc. 102 (1980) 7211–7218;
(b) A.E. Reed, F. Weinhold, J. Chem. Phys. 78 (1983) 4066–4073;
(c) A.E. Reed, R.B. Weinstock, F. Weinhold, J. Chem. Phys. 83 (1985) 735–746;
(d) A.E. Reed, L.A. Curtiss, F. Weinhold, Chem. Rev. 88 (1988) 899–926.
[9] (a) M. Casida, Time dependent density functional response theory for molecules, in: D.P. Chong (Ed.), Recent Advances in Density Functional Methods, World Scientific, Singapore, 1995;
(b) E.U.K. Gross, J.F. Dobson, M. Petersilka, in: R.F. Nalewajski (Ed.), Density Functional Theory, Springer Series Topics in Current Chemistry, Springer, Heidelberg, 1996.
[10] Y. Nie, Ph.D. Thesis, Universität Heidelberg, 2005.
[11] Y.S. Sohn, D.N. Hendrickson, H.B. Gray, J. Am. Chem. Soc. 93 (1971) 3603–3612.
[12] (a) G.M. Sheldrick, SHELXS86, University of Göttingen, Germany, 1986;
(b) G.M. Sheldrick, SHELXL97, University of Göttingen, Germany, 1997;
(c) G.M. Sheldrick, SHELXTL, Version 5.1, Program Package for Structure Solution and Refinement, Bruker Analytical X-ray Systems, Inc., Madison, WI, 1998.
[13] M.J. Frisch, G.W. Trucks, H.B. Schlegel, G.E. Scuseria, M.A. Robb, J.R. Cheeseman, V.G. Zakrzewski, J.A. Mongomery Jr., R.E. Stratmann, J.C. Burant, S. Dapprich, J.M. Millam, A.D. Daniels, K.N. Kudin, M.C. Strain, O. Farkas, J. Tomasi, V. Barone, M. Cossi, R. Cammi, B. Mennucci, C. Pomelli, C. Adamo, S. Clifford, J. Ochterski, G.A. Petersson, P.Y. Ayala, Q. Cui, K. Morokuma, P. Salvador, J.J. Dannenberg, D.K. Malick, A.D. Rabuck, K. Raghavachari, J.B. Foresman, J. Cioslowski, J.V. Oritz, A.G. Baboul, B.B. Stefanov, G. Liu, A. Liashenko, P. Piskorz, I. Komaromi, R. Gomperts, R.L. Martin, D.J. Fox, T. Keith, M.A. Al-Laham, C.Y. Peng, A. Nanayakkara, M. Challacombe, P.M.W. Gill, B. Johnson, W. Chen, M.W. Wong, J.L. Andres, C. Gonzalez, M. Head-Gordon, E.S. Replogle, J.A. Pople, GAUSSIAN 98 (Rev. A11), Gaussian, Inc., Pittsburgh, PA, 2001.
[14] A.J.H. Wachters, J. Chem. Phys. 52 (1970) 1033–1036.
[15] R. Krishnan, J.S. Binkley, R. Seeger, J.A. Pople, J. Chem. Phys. 72 (1980) 650–654.

[16] (a) The basis sets are available from the TURBOMOLE homepage http://www.turbomole.com via FTP Server Button in the subdirectory basen;
(b) A. Schäfer, C. Huber, R. Ahlrichs, J. Chem. Phys. 100 (1994) 5829–5835.

[17] D. Andrae, U. Häußermann, M. Dolg, H. Stoll, H. Preuß, Theor. Chim. Acta 77 (1990) 123–141.

[18] G. Schaftenaar, J.H. Noordik, MOLDEN: a pre- and post-processing program for molecular and electronic structures, J. Comput.-Aid. Mol. Des. (2000) 123.